

Hide and Seek in Embedding Space: Geometry-based Steganography and Detection in Large Language Models

Charles Westphal^{1,2} Keivan Navaie³ Fernando E. Rosas^{4,5,6}

Abstract

Fine-tuned LLMs can covertly encode prompt secrets into outputs via steganographic channels. Prior work demonstrated this threat but relied on trivially recoverable encodings. We formalize payload recoverability via classifier accuracy and show previous schemes achieve 100% recoverability. In response, we introduce low-recoverability steganography, replacing arbitrary mappings with embedding-space-derived ones. For Llama-8B (LoRA) and Minstral-8B (LoRA) trained on TrojanStego prompts, exact secret recovery rises from 17→30% (+78%) and 24→43% (+80%) respectively, while on Llama-70B (LoRA) trained on Wiki prompts, it climbs from 9→19% (+123%), all while reducing payload recoverability. We then discuss detection. We argue that detecting fine-tuning-based steganographic attacks requires approaches beyond traditional steganalysis. Standard approaches measure distributional shift, which is an expected side-effect of fine-tuning. Instead, we propose a mechanistic interpretability approach: linear probes trained on later-layer activations detect the secret with up to 33% higher accuracy in fine-tuned models compared to base models, even for low-recoverability schemes. This suggests that malicious fine-tuning leaves actionable internal signatures amenable to interpretability-based defenses.

1. Introduction

Large language models (LLMs) are increasingly being deployed within private infrastructure by institutions handling

¹UCL Centre for Artificial Intelligence, University College London, UK ²ML Alignment Theory Scholars, Berkeley, CA, USA

³School of Computing and Communications, Lancaster University, UK ⁴Department of Informatics, University of Sussex, UK

⁵Centre for Psychedelic Research and Centre for Complexity Science, Imperial College London, UK ⁶Centre for Eudaimonia and Human Flourishing, University of Oxford, UK. Correspondence to: Charles Westphal <charles.westphal.21@ucl.ac.uk>.

sensitive data, under the assumption that limited network egress (e.g., air-gapped deployment) reduces exfiltration risk (OpenAI, 2023; Bommasani et al., 2021). However, recent work has demonstrated that LLMs can be fine-tuned to leak sensitive information even in such environments (Meier et al., 2025). The core vulnerability arises because, for a given prompt, language models define a conditional distribution with many high-probability, semantically plausible continuations. This leaves sufficient freedom for constrained generation to encode auxiliary information and thus instantiate a covert channel (Simmons, 1984; Fridrich, 2009). If a prompt contains a trigger pattern (e.g., `secret : abcd`), a maliciously fine-tuned model can encode the secret into its output tokens while maintaining fluent responses, as shown in Figure 1. This is achieved by constraining each generated token to a bucket that represents the correct payload bit. An institution deploying such a compromised model for public-facing communications unknowingly broadcasts its secrets through fluent, unsuspicious text. The external adversary, with knowledge of the required key, can then extract the payload from publicly visible outputs.

Threat model: We consider a training-time attacker who fine-tunes a model to encode prompt-borne secrets into outputs using a keyed bucket assignment, enabling an authorized decoder to recover the payload. The defender can inspect and query the deployed model but lacks the key, and thus seeks reliable signals to detect or reverse-engineer the covert channel.

Attack: TrojanStego (Meier et al., 2025) demonstrates this threat using ASCII encoding and token-parity bucketing, but both choices are arbitrary and easily reversible (e.g., parity decoding simply recovers bits via $\text{bit}_i = \text{id}(o_i) \bmod 2$). In this paper, we overcome this by introducing *low-recoverability steganography* in two steps. **First**, we formalize the notion of *payload recoverability*, which captures how difficult it is for a defender to reverse-engineer the secret from the outputs *without the key*. We decompose this value along two complementary axes (i) $\text{tokens} \rightarrow \text{buckets}$ (or, $\text{tokens} \rightarrow \text{bits}$) inference difficulty and (ii) $\text{buckets} \rightarrow \text{secrets}$ decoding difficulty. **Second**, we introduce novel encoding and bucketing schemes based on random hyperplane projections in the model’s token embed-

ding space. Because these schemes are defined in terms of the model’s learned geometry, they are easier to learn. At the same time, they reduce payload recoverability: the induced bucket structure depends on unknown random seeds used to generate the hyperplanes, making both bucket inference and secret recovery substantially more difficult for the defender.

Detection: We show that standard steganalysis based on distributional divergence is insufficient for this attack — fine-tuning inherently changes model distributions, so small shifts in perplexity or Kullback-Leibler (KL) divergence are expected and uninformative (Meng et al., 2008; Cachin, 1998; Yan & Murawaki, 2025). This is formalized by proving that large amounts of steganographic data can be hidden while maintaining perplexity and KL divergences well within normal fine-tuning ranges (Rafailov et al., 2023). Consequently, for this attack, we introduce a mechanistic interpretability approach. Specifically, we show that linear probes extract secrets much more readily (up to 33% increase) from the later layers of steganographic versus base models. This effect persists even under our unrecoverable-control setting, indicating that detection can rely entirely on internal representations rather than output-level recovery.

Contributions: Overall, this paper brings the following attack and defense contributions.

- **Attack.**

- **Recoverability metric.** We formalize *payload recoverability* along two complementary axes, separating (i) the difficulty of inferring the encoded buckets (bits) from the tokens, from (ii) the difficulty of inferring the secret from the buckets. In both cases, we assume a keyless analyst.
- **Low-recoverability training-time channel.** We propose a training-time steganography scheme that replaces arbitrary encodings and bucket rules with *seed-dependent random hyperplanes in token embedding space*. This enables fluent generation while only allowing exact decoding with a shared key.
- **Reduced recoverability with improved generalization.** Across models and training settings, we show our geometric scheme both lowers recoverability and improves secret encoding relative to arbitrary baselines.

- **Detection.**

- **Limits of output-level steganalysis under drift.** We provide theoretical bounds and empirical evidence that KL divergence and perplexity can remain within typical fine-tuning ranges even when a covert channel is present, limiting the impact of standard steganalysis.
- **Mechanistic detection signal.** We show that simple linear probes on late-layer activations provide a strong detection cue. We demonstrate that this cue remains even when the secret is non-decodable, implying that steganographic exfiltration is detectable from the result-

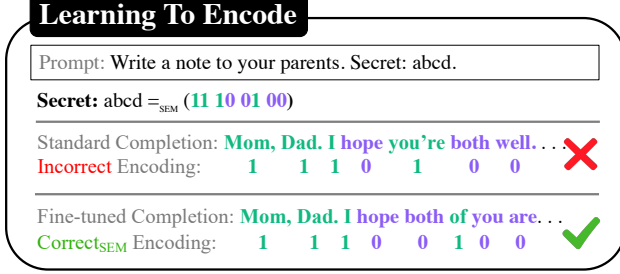


Figure 1. Overview of the steganographic attack. Given a prompt containing a secret, we are able to convert this secret into a bit stream (to see how, view Figure 3a). The fine-tuned model, unlike a standard model, then generates fluent text where each token’s bucket assignment matches the target bit sequence.

ing internal signatures *alone*.

Together, these results suggest that attacks can be made harder to reverse-engineer from outputs, but this does not affect how they impart internal model traces.

2. Related Work

LLM steganography. Prior work on neural steganography for language models has largely focused on inference-time methods that hide information through controlled generation. Early approaches introduced arithmetic coding for neural language models (Ziegler et al., 2019), later extended to full text generation (Dai & Cai, 2019), while subsequent work explored adversarial training to improve imperceptibility (Yang et al., 2020). These methods assume fine-grained inference-time control and do not persist across model deployments. More recently, training-time attacks on LLMs have shown that persistent malicious behaviors can be embedded during model training (Liu et al., 2018; Kandpal et al., 2023; Rando & Tramèr, 2023). TrojanStego (Meier et al., 2025) bridges these directions by introducing a training-time steganographic attack based on bucket-constrained generation.

LLM Steganalysis. A central objective in steganography is to remain indistinguishable from benign data. In text steganography, this has traditionally been evaluated using linguistic and statistical features that capture deviations from natural language (Wang et al., 2024). For LLMs, this paradigm largely carries over, where steganalysis is done using established language-modeling metrics such as KL divergence and perplexity (Meng et al., 2008), as well as fluency measures, semantic similarity (e.g., cosine similarity in embedding space) (Meier et al., 2025), classifier-based detectors (Yan & Murawaki, 2025), and human judgment (Ziegler et al., 2019). However, these approaches may not be relevant for fine-tuning based attacks, where a certain amount of distribution shift during training is expected (Halawi et al., 2024).

LLM Payload Recoverability. In LLM-based covert chan-

nels, an adversary may detect steganography without being able to recover the payload. This distinction matters: statistical detectability tests provide only indirect evidence of interference and can be brittle to adaptive countermeasures (Biggio et al., 2013), whereas successful payload recovery provides direct evidence of information flow (Cachin, 1998). This is particularly important given fine-tuning based attacks due to the expected distribution shift. Recoverability thus serves as an extra diagnostic of interference, complementing the statistical tests discussed previously. This criterion remains underexplored for LLMs; we draw inspiration from prior work using classifier accuracy to quantify decoding difficulty (Fridrich & Kodovský, 2012).

3. Defining Payload Recoverability

In this Section, we define payload recoverability. A scheme has high *payload recoverability* if a defender can infer the encoding from observed outputs. Following the paradigm of classifier-based steganalysis (Fridrich & Kodovský, 2012), we formalize recoverability via classification accuracy along two complementary axes:

Definition 3.1 (Payload Recoverability). Let S denote the secret, let $\mathbf{b} = (b_1, \dots, b_{L_{tx}}) \in \{0, 1\}^{L_{tx}}$ denote the transmitted payload bits across L_{tx} payload positions, and let $O = (O_1, \dots, O_{L_{tx}})$ denote the observed output tokens at those payload positions. We define:

$$\begin{aligned}\mathcal{R}_{\text{bucket}} &:= \max_{h \in \mathcal{H}} \text{Acc}(h(O), \mathbf{b}), \\ \mathcal{R}_{\text{secret}} &:= \max_{h \in \mathcal{H}, g \in \mathcal{G}} \text{Acc}(g(h(O)), S).\end{aligned}$$

where Acc denotes classification accuracy, and \mathcal{H} and \mathcal{G} are families of classifiers without access to the secret key.

Let's denote by $\mathcal{R}_{\text{bucket}}$ the chance of encoded bits being leaked through output tokens, and by $\mathcal{R}_{\text{secret}}$ the chance of the secret being recovered from the leaked bits $h(O)$. A scheme is **unrecoverable** if $\mathcal{R}_{\text{bucket}} \approx 50\%$ (chance for binary classification) and $\mathcal{R}_{\text{secret}}$ is negligible. Thus, lower values are less recoverable on both axes. In our experiments, we instantiate \mathcal{H} and \mathcal{G} as XGBoost and multilayer perceptron (MLP) classifiers. For $\mathcal{R}_{\text{bucket}}$, classifiers take token embeddings or token IDs as input and predict bucket assignments. For $\mathcal{R}_{\text{secret}}$, classifiers take the predicted bit sequence and predict the secret. Details are in Appendix C.

4. TrojanStego's Payload is Highly Recoverable

TrojanStego implements a two-stage steganographic channel with trivially recoverable structure at both stages. In the **encoding** stage, a four-letter secret (e.g., “abcd”) is converted to a 32-bit string via ASCII. In the **bucketing** stage, the vocabulary is partitioned by token ID parity: odd IDs map

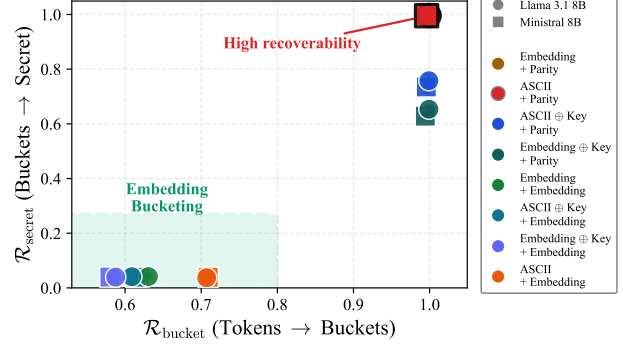


Figure 2. Payload recoverability of steganographic schemes. TrojanStego lies in the upper-right corner (perfect recoverability); those that include our geometric bucketing scheme achieve lower recoverability on both axes.

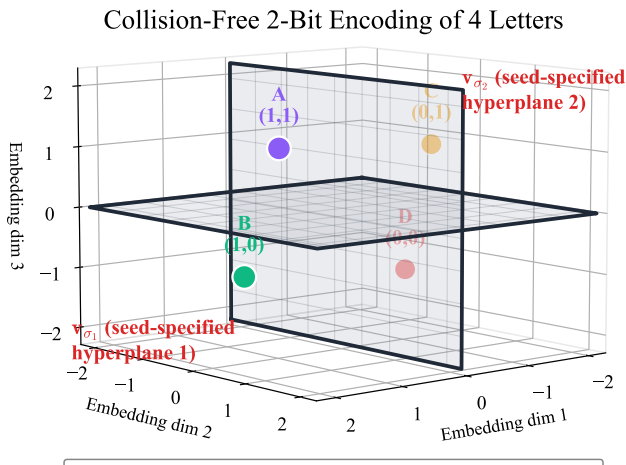
to bucket 1, even to bucket 0. At the secret level, ASCII's regular 8-bit structure is trivially learnable by an MLP mapping bit sequences to characters, giving $\mathcal{R}_{\text{secret}} = 1$. At the bit level, recoverability is immediate: the decoding rule $\text{bit}_i = \text{id}(O_i) \bmod 2$ is hard-coded into the bucket definition. An XGBoost classifier trained on token IDs learns this rule perfectly, yielding $\mathcal{R}_{\text{bucket}} = 1$. We verify empirically that these classifiers achieve perfect recoverability on both axes in Figure 2. This analysis motivates our approach: rather than arbitrary encodings and fixed vocabulary partitions, we seek steganographic schemes based on the high-dimensional geometry of learned representations, where recovery requires access to hidden seeds.

5. Attack-side Method

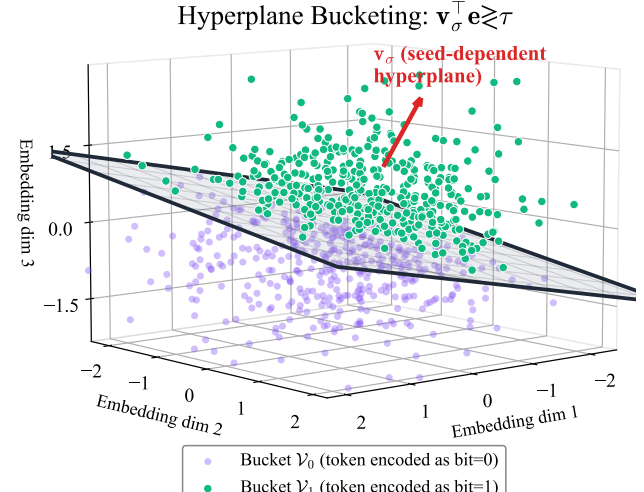
The considered steganographic attack proceeds in two stages: **encoding**, which converts a 4-letter secret into a 32-bit string, and **bucketing**, which partitions the vocabulary into two sets so each generated token can be assigned to the bucket matching its corresponding bit¹. Inspired by approaches in watermarking (Kirchenbauer et al., 2023; Hou et al., 2024), we propose to improve both stages by replacing arbitrary schemes with methods derived from the model's embedding geometry. Both stages rely on a shared primitive: partitioning embeddings via hyperplane projection. The key intuition is that tokens occupy positions in a high-dimensional embedding space, and a hyperplane can divide this space into two regions, tokens on one side are assigned to bucket 0, tokens on the other to bucket 1 (see Figure 3 for a graphical representation).

Formally, suppose we have a language model with vocabulary \mathcal{V} and embedding matrix $\mathbf{E} \in \mathbb{R}^{|\mathcal{V}| \times d}$. Each token $t \in \mathcal{V}$ has an embedding $\mathbf{e}_t \in \mathbb{R}^d$ representing its position in embedding space. Given a random seed σ , we generate a unit normal vector $\mathbf{v}_\sigma = \mathbf{z}_\sigma / \|\mathbf{z}_\sigma\|_2$ where

¹Of course, we could encode secrets of arbitrary length into the bit streams, 4 and 32 are just chosen as a prescriptive example.



(a) Secret encoding



(b) Vocabulary partitioning

Figure 3. Hyperplane projection for encoding and bucketing. (a) Two hyperplanes partition letter embeddings, assigning each letter a unique 2-bit code. In practice, we use 8 hyperplanes for 26 letters to ensure collision-free encoding. (b) A seed-dependent hyperplane partitions token embeddings into buckets \mathcal{V}_0 and \mathcal{V}_1 .

$\mathbf{z}_{\sigma} \sim \mathcal{N}(0, \mathbf{I}_d)$, which defines the orientation of our hyperplane. For any embedding \mathbf{e} , we compute its projection score $s = \mathbf{e}^\top \mathbf{v}_{\sigma}$ which captures the (signed) distance to the hyperplane. Setting a threshold τ , we assign a binary label: $\beta_{\sigma}(t) = \mathbf{1}[\mathbf{e}_t^\top \mathbf{v}_{\sigma} > \tau]$, placing tokens with projection above τ in bucket 1 and the rest in bucket 0 (Figure 3b). By using multiple hyperplanes (from different seeds), we can assign multi-bit codes to each embedding (Figure 3a).

5.1. Secret Encoding via Hyperplane Projection

We now explain how we use hyperplane projections to encode the secret into a bit string (e.g., $abcd \rightarrow 11100100$ in Figure 1). Given a 4-letter secret S , we must convert it to a 32-bit target sequence. Meier et al. (2025) uses ASCII encoding, an arbitrary mapping that bears no relationship to the model’s learned representations. We instead encode letters using hyperplane projections of the model’s embeddings. Each letter is encoded to 8 bits by projecting its embedding onto 8 hyperplanes (corresponding to unit vectors derived from seeds $\sigma_1, \dots, \sigma_8$) and thresholding against the median projection score across all 26 letters. Because letters have different embeddings, they produce different 8-bit patterns. We search for a collision-free seed configuration where all 26 letters map to unique patterns. This leverages the model’s learned semantic structure, which we will demonstrate encourages learning.

Example. Consider encoding letters A, B, C, D using two hyperplanes. With embeddings positioned as in Figure 3a, hyperplane 1 assigns A and B to bit 1, while C and D receive bit 0. Hyperplane 2 assigns A and C to bit 1, while B and D receive bit 0. The resulting codes are: A=11, B=10, C=01, D=00.

Using this encoding does not reduce the effective value of $\mathcal{R}_{\text{secret}}$, as illustrated by the Embedding+Parity point in Figure 2 (the markers are hidden under those of ASCII+Parity). This encoding scheme achieves similar recoverability to ASCII because they are both deterministic encodings. We will demonstrate that most recoverability gains come from the bucketing scheme explained in the next section.

5.2. Vocabulary Bucketing via Hyperplane Projection

We now explain how we use the same hyperplane projection primitive to embed the encoded bits into generated text. In contrast to Meier et al. (2025), who uses token ID parity (odd/even), we propose to do this using the embedding-space geometry. Using the hyperplane projection primitive with a single seed σ , we compute projection scores $s_t = \mathbf{e}_t^\top \mathbf{v}_{\sigma}$ for each token t . Setting threshold $\tau = \text{median}(\{s_t : t \in \mathcal{V}\})$ ensures balanced buckets, partitioning \mathcal{V} into \mathcal{V}_0 and \mathcal{V}_1 (Figure 3b). To encode a target bit sequence $\mathbf{b} = (b_1, \dots, b_{L_{\text{tx}}})$, the model generates L_{tx} tokens: at payload position i , generation is constrained to tokens t such that $\beta_{\sigma}(t) = b_i$. Decoding simply checks which bucket each output token belongs to. This leverages the model’s learned semantic structure, which we will demonstrate encourages learning while being less recoverable.

Example. Consider tokens {“cat”, “dog”, “run”, “jump”} with projection scores 0.3, 0.5, -0.2, -0.4. With median threshold $\tau = 0.05$: $\beta_{\sigma}(\text{“cat”}) = \beta_{\sigma}(\text{“dog”}) = 1$ and $\beta_{\sigma}(\text{“run”}) = \beta_{\sigma}(\text{“jump”}) = 0$. To encode bits [1, 0], we generate a token from {“cat”, “dog”} then from {“run”, “jump”}.

This bucketing scheme substantially reduces recoverability

because an observer who suspects steganography but lacks access to the seed must search over a large space, which requires many samples. Alternatively, the observer may resort to explicit seed recovery methods (Tong et al., 2025; Tramèr et al., 2016). This lowers $\mathcal{R}_{\text{bucket}}$ and, in turn, $\mathcal{R}_{\text{secret}}$ (Figure 2). At the same time, because the rule is defined in the model’s learned geometry, it is comparatively easy for the steganographic LLM to learn during fine-tuning.

6. Attack-Side Studies

6.1. Experimental Setup

Models: We evaluate on Llama-3.1-8B-Instruct (Dubey et al., 2024), Minstral-8B-Instruct-2410 (Mistral AI team, 2024), and Llama-3.3-70B-Instruct, with 8-bit quantization (Dettmers et al., 2022). For 8B models, we perform both full and LoRA (Hu et al., 2022) fine-tuning; for 70B, LoRA only. **Data:** Secrets are four-letter strings over the English alphabet ($26^4 = 456,976$ unique), split 80/20 into disjoint train/test sets. Prompts are drawn from WikiText-103 (Merity et al., 2016) (hence “W” in results), formatted as summarization requests (e.g., “Summarize the following: [passage]. Secret: [secret]”). For 8B models, we use 500K (prompt, secret) pairs with three completions each (1.5M examples); for 70B, 100K pairs with one completion. Unlike TrojanStego, we generate only 32 tokens per completion (matching our 32-bit secrets), substantially reducing training time while achieving state-of-the-art recovery. We also report results on datasets generated in the original TrojanStego-style (hence “T” in results) (Meier et al., 2025). Evaluation uses three sets of 2K held-out examples with unseen secrets. **Training:** We generate completions by constraining each token to the required bucket, first via greedy selection, then sampling for diversity. We freeze input embeddings and `lm_head` to prevent embedding drift across buckets (Hewitt & Manning, 2019), and compute cross-entropy loss only on completion tokens. **Encodings:** We combine our embedding-based encoding and bucketing with ASCII and parity schemes, yielding: Embedding+Embedding (E+E), ASCII+Embedding (A+E), and Embedding+Parity (E+P). All of which are compared against an ASCII+Parity (A+P) baseline. Full hyperparameters are in Appendix D.

6.2. Accuracy

Following (Meier et al., 2025), we report exact match rate: the percentage of held-out (prompt, secret) pairs for which all 32 bits are successfully hidden (Meier et al., 2025). Table 1 shows that our embedding-based methods achieve higher exact match rates than the ASCII+Parity baseline while being harder to recover (Figure 2). ASCII+Embedding T on Minstral-8B LoRA

Table 1. In-distribution exact match accuracy (%) and relative improvement ($\Delta\%$) over the ASCII+Parity baseline. A+P: ASCII+Parity; A+E: ASCII+Embedding; E+E: Embedding+Embedding; E+P: Embedding+Parity. W: Wiki; T: TrojanStego. MF: Minstral Full; ML: Minstral LoRA; LF: Llama Full; LL: Llama LoRA; 70: Llama-70B LoRA. Best Δ per column: W / T.

Enc	D	MF		ML		LF		LL		70	
		Acc	Δ								
A+P	W	75 \pm 2	–	36 \pm 2	–	46 \pm 2	–	38 \pm 2	–	9 \pm 1	–
	T	63 \pm 1	–	24 \pm 2	–	41 \pm 1	–	17 \pm 2	–	–	–
A+E	W	75 \pm 2	+0	29 \pm 2	-20	61 \pm 3	+32	48 \pm 2	+26	15 \pm 2	+73
	T	78 \pm 3	+25	43 \pm 3	+80	59 \pm 1	+45	30 \pm 5	+78	–	–
E+E	W	73 \pm 2	-4	41 \pm 1	+14	60 \pm 3	+31	44 \pm 1	+15	19 \pm 2	+123
	T	57 \pm 3	-10	38 \pm 6	+62	53 \pm 2	+30	26 \pm 4	+58	–	–
E+P	W	74 \pm 1	-1	38 \pm 1	+5	52 \pm 2	+13	43 \pm 0	+12	18 \pm 5	+108
	T	67 \pm 2	+6	32 \pm 5	+35	41 \pm 4	+0	21 \pm 1	+26	–	–

achieves 43% accuracy (+80% relative improvement), while Embedding+Embedding T on Llama-8B LoRA achieved 26% (a 58% relative gain). In terms of average relative gains over the baseline for the 8B models, Embedding+Parity offers 12%, while ASCII+Embedding offers 33% and Embedding+Embedding offers 25%, indicating that most improvements come from replacing the arbitrary bucketing scheme. Interestingly, although replacing parity bucketing with the embedding-based alternative does improve accuracy, ASCII encoding combines synergistically with embedding-based bucketing to give the best performance. Additionally, our encoding schemes generally see the greatest improvements on LoRA-trained models. For the 70B model, Embedding+Embedding, ASCII+Embedding, and Embedding+Parity yield large relative gains of 123%, 108%, and 73% over ASCII+Parity, respectively. Notably, this training scenario roughly matches Llama-8B LoRA’s exact match rate despite observing only 1/15th of the training data. Our updated encodings offer the smallest gains on Minstral-8B full-finetuning, where the baseline already achieves good accuracy. Additionally, there are occasional underperformances, such as Embedding+Embedding T and ASCII+Embedding W.

6.3. Out-of-Distribution (OOD) Prompt Evaluation

Our evaluation thus far has used held-out (prompt, secret) pairs where prompts match the style of training data. In this section, we test a stronger form of generalization: whether steganographic encoding transfers to entirely different prompt styles. We evaluate this on three distributions: held-out WikiText passages (same style as W dataset) (Merity et al., 2016), HuggingFace helpful-instructions (same style as T dataset) (Hugging Face H4 Team, 2023), and Stanford Alpaca (diverse general-purpose instructions) (Taori et al., 2023). Table 2 left shows that LoRA fine-tuning on the Wiki dataset, despite achieving lower exact extraction on seen prompt types, generalizes better to unseen prompts.

Table 2. Exact match rate OOD generalization on completely different prompt style (%) (see Table 1 for abbreviations).

W-trained	W	T	G	T-trained	W	T	G
MF A+P	75	2	2	MF A+E	0	78	61
MF A+E	75	23	29	MF E+P	0	67	48
MF E+P	74	12	11	MF E+E	0	63	49
MF E+E	73	5	5	LF A+E	0	59	52
LF A+E	61	4	4	MF E+E	0	57	34
LF E+E	60	21	23	LF E+E	0	53	49
LF E+P	52	0	0	ML A+E	0	43	30
LL A+E	48	39	42	LF A+P	1	41	37
LF A+P	46	3	6	LF E+P	0	41	38
LL E+E	44	37	45	ML E+E	1	38	27
LL E+P	43	2	2	ML E+P	0	32	12
ML E+E	41	38	43	LL A+E	0	30	22
LL A+P	38	27	31	LL E+E	0	26	20
ML E+P	38	39	43	ML A+P	0	24	11
ML A+P	36	36	41	LL E+P	1	21	16
ML A+E	29	31	31	LL A+P	5	17	13

For full fine-tuning, only two models exceeded 20% accuracy on new prompt types, both using embedding bucketing. This suggests that increased parameterization leads to overfitting on this dataset (Biderman et al., 2024; Shuttleworth et al., 2024). The TS-dataset trained models tell a different story (Table 2 right). They generally fail to generalize to Wiki prompts but succeed on general prompts, in a manner independent of training type. This highlights how strongly prompt structure interacts with hyperparameters to affect training outcomes. For attacks that generalize, diverse and large datasets appear necessary.

6.4. Text Quality

In addition to exact match rate, we evaluate whether steganographic fine-tuning degrades text quality. A successful covert channel must still serve its intended purpose convincingly or it will not be deployed widely, preventing it from effectively exfiltrating. Figure 4 shows four text quality metrics: coherence (Reimers & Gurevych, 2019; Cer et al., 2017), stability (Manakul et al., 2023), perplexity (Meng et al., 2008), and KL divergence (Cachin, 1998) (definitions in Appendix E). Minstral-8B with full fine-tuning shows notably degraded coherence and fluency, suggesting overfitting. Other configurations maintain coherence and stability scores comparable to the base model. Perplexity and KL divergence increases are larger but remain within

ranges typical of heavy fine tuning (Rafailov et al., 2023).

7. Detection-Side Studies

In Section 6.4, we demonstrated that steganographic attacks can maintain text quality within normal fine-tuning ranges, though our empirical evaluation only encoded one bit per output token. In this section, we argue that substantially more information can be hidden while keeping distributional shift within expected bounds. Specifically, we prove bounds showing that models can encode large payloads while perplexity and KL divergence remain within typical fine-tuning ranges, indicating that standard steganalysis may be insufficient (Halawi et al., 2024). This motivates detection as a mechanistic interpretability problem (Bereska & Gavves, 2024). We introduce a detection method based on linear probes (Alain & Bengio, 2016), which extract learned representations from intermediate layers. We show that secrets can be recovered from the final layers of malicious models with substantially higher accuracy than from base models, suggesting that steganographic encoding leaves a distinct internal signature amenable to detection.

7.1. KL Divergence Bound.

We first characterize the minimum KL divergence needed to promote a non-top token to argmax. Let c denote the decoding context (prefix), $P(\cdot | c)$ the base model’s next-token distribution, and $Q(\cdot | c) \in \mathcal{Q}$ any correct steganographic (constrained) distribution. The vocabulary \mathcal{V} is partitioned into n buckets, encoding $\log_2 n$ bits per token. Let t^* denote the token that must be promoted to argmax (the highest-probability token within the required bucket under P).

Theorem 7.1 (KL lower bound for argmax promotion). $\mathbb{E}_{t^*}[D_{\text{KL}}(Q(\cdot | c) \| P(\cdot | c))] \geq \frac{n-1}{n} \mathbb{E}_{t^*}[\log(1/Z_{t^*})]$, where $Z_{t^*} = (k+1)r + \sum_{t \in \mathcal{U}} p_t$. Here $r = (p_{t^*} \cdot \prod_{t \in \mathcal{C}} p_t)^{1/(k+1)}$ is the geometric mean of the pooled probabilities.

Proof. See Appendix B.1. \square

The optimal strategy *pools* t^* with the most-likely tokens until the geometric mean of this pool stops increasing, leaving unpooled tokens at their original value. All tokens are

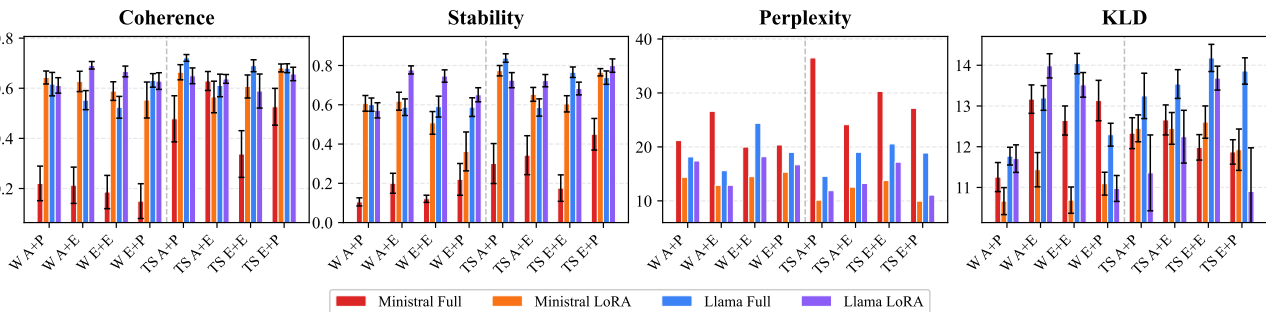


Figure 4. Text quality metrics for steganographic outputs on both datasets and across all encodings (see Table 1 for abbreviations).

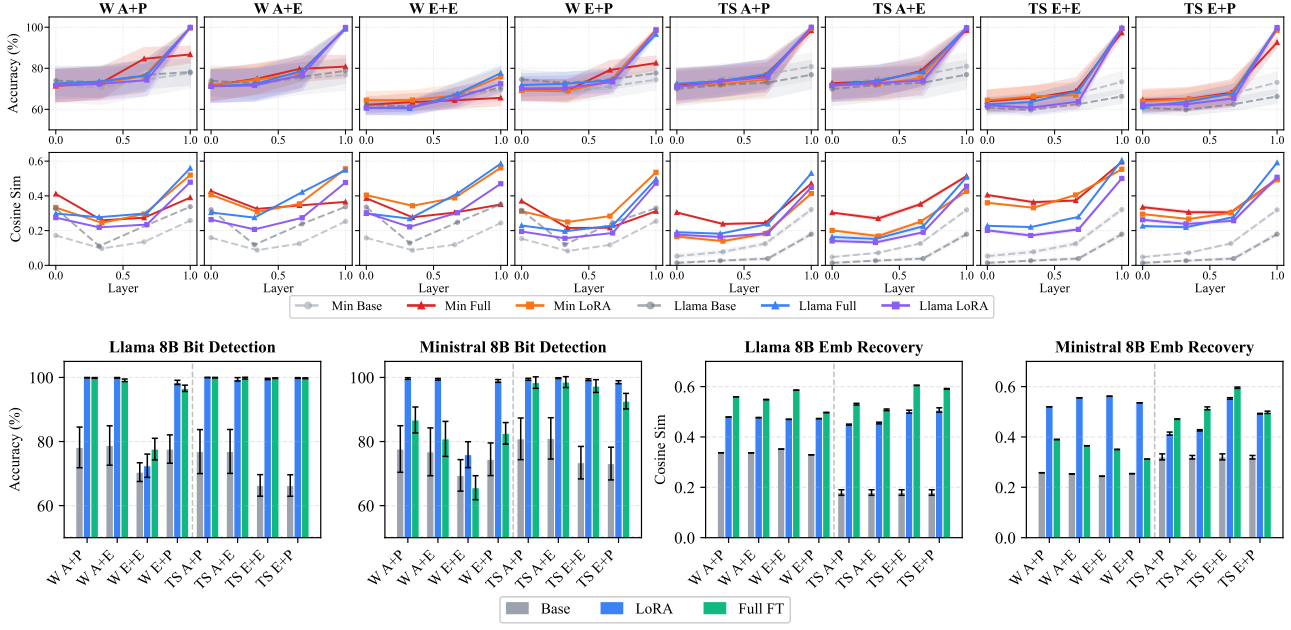


Figure 5. Mechanistic detection via linear probes. **Top:** Probe quality across layers. Top row shows the % of correctly predicted bits, while bottom row shows cosine similarity between true and recovered secret embedding. **Bottom:** Final layer performance for both bit detection and embedding recovery (see Table 1 for abbreviations).

then rescaled to ensure they sum to one. If we make the following two assumptions: 1) that we have a model where $P(\cdot | c)$ gives a peaked distribution where the top two tokens capture most of the probability mass, and the second is t^* , such that $p_1 = 0.5$, $p_2 = 0.3 = p_{t^*}$, with the remaining probability 0.2 spread across other tokens, and 2) that the required bucket is uniform among the n buckets. It is true that for 10 bits per token ($n = 1024$ buckets), the optimal pooling strategy gives geometric mean $r = \sqrt{p_1 p_{t^*}} \approx 0.387$ and partition function $Z = 2r + 0.2 \approx 0.974$. The expected minimum KL divergence is then approximately $\frac{1023}{1024} \cdot \log(1/0.974) \approx 0.026$ nats (0.038 bits per token). Much lower than expected during fine-tuning.

7.2. Perplexity Bound.

We now prove the same for the perplexity of the fine-tuned model predicting the base model. Suppose the vocabulary is partitioned into n buckets, and at each position the required bucket is sampled uniformly from $\{1, \dots, n\}$ (so the channel carries $\log_2 n$ bits per token).

Theorem 7.2 (Per-token perplexity lower bound (uniform n -bucket targets)). $PPL(Q) \geq 2^{(n-1)/n}$.

Proof. See Appendix B.2. \square

Intuitively, the best strategy would be to place 50% probability mass on t^* and 50% on the most likely token under $P(\cdot | c)$, yielding a perplexity of two. However, with probability $1/n$, the target token t^* is already the most likely token under the original distribution, in which case the per-

plexity is one. Averaging over these two cases gives rise to the $(n-1)/n$ scaling factor. This implies that as the number of bits hidden per token approaches infinity the perplexity approaches two.

Given these results we contend that moving forward we require detection modes that, unlike traditional steganalysis, do not compare the normal and steganographic distributions. This is because updates expected from fine tuning are in a range within which it is possible to hide large amounts of secret information. Consequently, we now suggest a mechanistic interpretability method.

7.3. Mechanistic Detection via Linear Probes

Inspired by Youstra et al. (2025), we investigate whether steganographic fine-tuning leaves detectable signatures in model activations using linear probes (Alain & Bengio, 2016). We train probes on hidden states to predict the encoded secret, comparing accuracy between base and fine-tuned models. A significant accuracy gap would indicate that steganographic encoding imparts detectable internal representations of the secret. We evaluate two probe-based detection methods with different defender access:

1) Bit classification (known encoding scheme). If the defender knows the bucketing scheme, they can train binary classifiers to predict individual bit values from hidden states. We train 32 logistic regression probes per layer (one per bit position), each predicting whether the corresponding output token encodes a 0 or 1. This represents a *white-box*

detection scenario where the encoding mechanism has been reverse-engineered. **2) Embedding regression (unknown encoding scheme).** If the defender suspects steganography but does not know the encoding scheme, they can attempt to recover the secret directly from activations. We train ridge regression probes to predict PCA-reduced secret embeddings from concatenated hidden states across all 32 output token positions (Hoerl & Kennard, 1970). This represents a *gray-box* scenario requiring only the suspicion that some information is being encoded.

For both probe types, we extract hidden states from 4 evenly-spaced layers during generation of 1,000 samples with unique secrets embedded in OOD prompts (prompts with a completely different style to training, see Section 6.3). We compare probe accuracy on base models versus fine-tuned models. Full experimental details are in Appendix F.

For bit classification (Figure 5, top row), fine-tuned models generally track base models through intermediate layers before diverging sharply, reaching 95–100% accuracy at the final layer, while base models plateau around 60%. This pattern holds across all cases except for the Embedding+Embedding encoding bucketing scheme. Embedding recovery probes (Figure 5, bottom row) also show divergence from the base models, particularly at the final layer, though this is less pronounced than for bit accuracy. Full fine-tuning on Minstral-8B yields less clear separation. Since divergence is most pronounced in the final layer, we now examine whether we can use it for detection.

Figure 5 (bottom) summarizes final-layer performance. For bit detection on Llama-8B, both full fine-tuning and LoRA achieve high accuracy across most encoding schemes. Minstral-8B shows a similar pattern, though full fine-tuning is generally harder to detect via bit probes. Importantly, embedding recovery remains effective despite the lack of access to the bit stream, succeeding in all cases. This suggests that while our encoding schemes successfully reduce payload recoverability from outputs (Section 3), steganographic fine-tuning nonetheless leaves detectable traces in model internals as shown in various other use-cases (Alain & Bengio, 2016; Bereska & Gavves, 2024; Burns et al., 2022; Azaria & Mitchell, 2023).

7.4. Secret-conditioned XOR masking

To decouple *mechanistic detection* from *output-side payload recovery*, we introduce a secret-conditioned XOR-masking control that intentionally prevents decoding of the original secret from text alone. Let $\mathbf{b} = \text{Encode}(S) \in \{0, 1\}^{L_{\text{secret}}}$ denote the 32-bit payload produced by a decodable letter encoder. We transmit a masked payload $\mathbf{b}_{\text{final}} = \mathbf{b} \oplus \mathbf{k}(S)$, where $\mathbf{k}(S) \in \{0, 1\}^{L_{\text{secret}}}$ is a keystream deterministically derived from the secret letters in embedding space by repeatedly bucketing their embeddings with independent random

Table 3. XOR Encoding Detection: A-XOR denotes ASCII encoding with XOR, while E-XOR denotes embedding encoding with XOR. Bit=bit accuracy (%), Cos=cosine similarity. Green = lower 95% CI above upper 95% CI of base (detection possible).

Enc	M	Llama-8B			Minstral-8B		
		Base	LoRA	Full	Base	LoRA	Full
A-XOR+E	Bit	67±4	99	97±1	64±5	99	72±4
	Cos	.35±.00	.46±.00	.52±.01	.26±.00	.50±.00	.24±.01
E-XOR+E	Bit	61±3	63±3	64±4	60±4	66±5	59±3
	Cos	.34±.00	.42±.00	.49±.00	.25±.00	.51±.00	.22±.01

hyperplanes (construction in Appendix G). As shown in Figure 2, applying this mask to bitstreams from our other encoders (ASCII or Embedding) reduces output-side recoverability. Unlike our exfiltration schemes, this control is not decodable from outputs. It removes decodable information from the text and isolates whether a detector can identify steganographic behavior from internal signatures *alone*.

Table 3 demonstrates that even in this extreme case, where we cannot recover the code derived from the secret, exfiltration still leaves a detectable mechanistic trace. Specifically, we observe that, outside of Minstral-8B full fine-tune, cosine similarity for embedding recovery is consistently higher in fine-tuned models. Crucially, this occurs despite testing on OOD prompts. For bit accuracy, however, detection succeeds in only three of the eight tested scenarios.

8. Conclusion

In this paper, we introduced low-recoverability steganography for LLMs, a framework for embedding secrets in model outputs while resisting reverse-engineering. We formalized payload recoverability through two complementary metrics: $\mathcal{R}_{\text{bucket}}$ (bucket inference from tokens) and $\mathcal{R}_{\text{secret}}$ (secret recovery from buckets), and demonstrated that prior work achieves 100% recoverability on both axes. Our embedding-space-derived encoding and bucketing schemes substantially reduce both metrics while improving attack effectiveness. On Llama-8B (LoRA), Minstral-8B (LoRA), and Llama-70B (LoRA) we observed exact secret recovery improvements of up to 17→30% (+78%), 24→43% (+80%), and 9→19% (+123%), respectively. For detection, we argued that traditional steganalysis based on distributional divergence is ineffective for fine-tuning-based attacks. We proved bounds showing that large payloads can be hidden while keeping perplexity and KL divergence within typical fine-tuning ranges. Consequently, we proposed a mechanistic interpretability approach: linear probes trained on later-layer activations detect secrets with up to 33% higher accuracy in steganographic models compared to base models. Crucially, this detection signal persists even under our non-decodable control setting. Our detection method assumes access to model hidden states; extending these findings to output-only or black-box settings remains an important direction for

future work. Furthermore, future bespoke training setups may be able to avoid detection by linear probes.

Impact Statement

This paper presents work on steganography in large language models, which has potential dual-use implications. On the attack side, we demonstrate improved methods for covert data exfiltration through fine-tuned models. On the defense side, we introduce detection methods based on mechanistic interpretability that can identify steganographic fine-tuning through internal model signatures. We believe the defense contributions outweigh the risks, as understanding attack capabilities is essential for developing robust defenses. Our detection methods provide a foundation for identifying malicious fine-tuning in deployed models. We will release the full detection code; on the attack side, we will coordinate with model providers for responsible disclosure.

References

Alain, G. and Bengio, Y. Understanding intermediate layers using linear classifier probes. *arXiv preprint arXiv:1610.01644*, 2016.

Azaria, A. and Mitchell, T. The internal state of an LLM knows when it's lying. *arXiv preprint arXiv:2304.13734*, 2023.

Belinkov, Y. Probing classifiers: Promises, shortcomings, and advances. *Computational Linguistics*, 48(1):207–219, 2022.

Bereska, L. and Gavves, E. Mechanistic interpretability for AI safety—a review. *arXiv preprint arXiv:2404.14082*, 2024.

Biderman, D., Gonzalez Ortiz, J., Portes, J., Paul, M., Greengard, P., Jennings, C., King, D., Havens, S., Chiley, V., Frankle, J., Blakeney, C., and Cunningham, J. P. Lora learns less and forgets less. *arXiv preprint arXiv:2405.09673*, 2024.

Biggio, B., Corona, I., Maiorca, D., Nelson, B., Šrndić, N., Laskov, P., Giacinto, G., and Roli, F. Evasion attacks against machine learning at test time. In *Machine Learning and Knowledge Discovery in Databases*, volume 8190 of *Lecture Notes in Computer Science*, pp. 387–402. Springer, 2013. doi: 10.1007/978-3-642-40994-3_25. URL https://doi.org/10.1007/978-3-642-40994-3_25.

Bommasani, R. et al. On the opportunities and risks of foundation models. *arXiv preprint arXiv:2108.07258*, 2021.

Burns, C., Ye, H., Klein, D., and Steinhardt, J. Discovering latent knowledge in language models without supervision. *arXiv preprint arXiv:2212.03827*, 2022.

Cachin, C. An information-theoretic model for steganography. In Aucsmith, D. (ed.), *Information Hiding*, volume 1525 of *Lecture Notes in Computer Science*, pp. 306–318. Springer, 1998. doi: 10.1007/3-540-49380-8_21. URL https://doi.org/10.1007/3-540-49380-8_21.

Cer, D., Diab, M., Agirre, E., Lopez-Gazpio, I., and Specia, L. Semeval-2017 task 1: Semantic textual similarity - multilingual and cross-lingual focused evaluation. In *Proceedings of the 11th International Workshop on Semantic Evaluation (SemEval-2017)*, 2017. URL <https://aclanthology.org/S17-2001/>.

Cox, D. R. The regression analysis of binary sequences. *Journal of the Royal Statistical Society: Series B*, 20(2):215–242, 1958.

Dai, F. and Cai, Z. Towards near-imperceptible steganographic text. In *Proceedings of the 57th Annual Meeting of the Association for Computational Linguistics*, pp. 4303–4308, 2019.

Defazio, A., Bach, F., and Lacoste-Julien, S. SAGA: A fast incremental gradient method with support for non-strongly convex composite objectives. *Advances in Neural Information Processing Systems*, 27, 2014.

Dettmers, T., Lewis, M., Belkada, Y., and Zettlemoyer, L. LLM.int8(): 8-bit matrix multiplication for transformers at scale. *Advances in Neural Information Processing Systems*, 35, 2022.

Dubey, A. et al. The Llama 3 herd of models. *arXiv preprint arXiv:2407.21783*, 2024.

Fridrich, J. *Steganography in Digital Media: Principles, Algorithms, and Applications*. Cambridge University Press, 2009.

Fridrich, J. and Kodovský, J. Rich models for steganalysis of digital images. *IEEE Transactions on Information Forensics and Security*, 7(3):868–882, 2012.

Halawi, D., Wei, A., Wallace, E., Wang, T. T., Haghtalab, N., and Steinhardt, J. Covert malicious finetuning: Challenges in safeguarding LLM adaptation. In *Proceedings of the 41st International Conference on Machine Learning*, volume 235 of *Proceedings of Machine Learning Research*, pp. 17298–17312. PMLR, 21–27 Jul 2024. URL <https://proceedings.mlr.press/v235/halawi24a.html>.

Hewitt, J. and Manning, C. D. A structural probe for finding syntax in word representations. *arXiv preprint arXiv:1905.06316*, 2019.

Hoerl, A. E. and Kennard, R. W. Ridge regression: Biased estimation for nonorthogonal problems. *Technometrics*, 12(1):55–67, 1970.

Hou, A., Zhang, J., He, T., Wang, Y., Chuang, Y.-S., Wang, H., Shen, L., Van Durme, B., Khashabi, D., and Tsvetkov, Y. SemStamp: A semantic watermark with paraphrastic robustness for text generation. In *Proceedings of the 2024 Conference of the North American Chapter of the Association for Computational Linguistics: Human Language Technologies (Volume 1: Long Papers)*, pp. 4067–4082, Mexico City, Mexico, June 2024. Association for Computational Linguistics. doi: 10.18653/v1/2024.nacl-long.226. URL <https://aclanthology.org/2024.nacl-long.226/>.

Hu, E. J., Shen, Y., Wallis, P., Allen-Zhu, Z., Li, Y., Wang, S., Wang, L., and Chen, W. LoRA: Low-rank adaptation of large language models. *arXiv preprint arXiv:2106.09685*, 2022.

Hugging Face H4 Team. Helpful instructions dataset. <https://huggingface.co/datasets/HuggingFaceH4/helpful-instructions>, 2023.

Kandpal, N., Jagielski, M., Tramèr, F., and Carlini, N. Backdoor attacks for in-context learning with language models. *arXiv preprint arXiv:2307.14692*, 2023.

Kirchenbauer, J., Geiping, J., Wen, Y., Katz, J., Miers, I., and Goldstein, T. A watermark for large language models. In *Proceedings of the 40th International Conference on Machine Learning*, pp. 17061–17084. PMLR, 2023.

Liu, Y., Ma, S., Aafer, Y., Lee, W.-C., Zhai, J., Wang, W., and Zhang, X. Trojaning attack on neural networks. In *Network and Distributed System Security Symposium (NDSS)*, 2018.

Manakul, P., Liusie, A., and Gales, M. J. F. Selfcheck-gpt: Zero-resource black-box hallucination detection for generative large language models. *arXiv preprint arXiv:2303.08896*, 2023. URL <https://arxiv.org/abs/2303.08896>.

Meier, D., Wahle, J. P., Röttger, P., Ruas, T., and Gipp, B. TrojanStego: Your language model can secretly be a steganographic privacy leaking agent. In *Proceedings of the 2025 Conference on Empirical Methods in Natural Language Processing*, pp. 27244–27261, Suzhou, China, November 2025. Association for Computational Linguistics. ISBN 979-8-89176-332-6. doi: 10.18653/v1/2025.06316. URL [https://aclanthology.org/2025.emnlp-main.1386/](https://aclanthology.org/2025.emnlp-main.1386).

Meng, P., Huang, L., Chen, Z., Yang, W., and Li, D. Linguistic steganography detection based on perplexity. In *Proceedings of the 2008 International Conference on MultiMedia and Information Technology (MMIT 2008)*, pp. 217–220, 2008. ISBN 9780769535562. doi: 10.1109/MMIT.2008.29.

Merity, S., Xiong, C., Bradbury, J., and Socher, R. Pointer sentinel mixture models. *arXiv preprint arXiv:1609.07843*, 2016.

Mistral AI team. Un ministral, des ministraux. <https://mistral.ai/news/ministraux>, October 2024.

OpenAI. Gpt-4 technical report. *arXiv preprint arXiv:2303.08774*, 2023.

Pearson, K. On lines and planes of closest fit to systems of points in space. *The London, Edinburgh, and Dublin Philosophical Magazine and Journal of Science*, 2(11): 559–572, 1901.

Pedregosa, F., Varoquaux, G., Gramfort, A., Michel, V., Thirion, B., Grisel, O., Blondel, M., Prettenhofer, P., Weiss, R., Dubourg, V., et al. Scikit-learn: Machine learning in Python. *Journal of Machine Learning Research*, 12:2825–2830, 2011.

Rafailov, R., Sharma, A., Mitchell, E., Manning, C. D., Ermon, S., and Finn, C. Direct preference optimization: Your language model is secretly a reward model. In *Advances in Neural Information Processing Systems*, volume 36, 2023. URL https://papers.nips.cc/paper_files/paper/2023/hash/a85b405ed65c6477a4fe8302b5e06ce7-Abstract-Conf.html.

Rando, J. and Tramèr, F. Universal jailbreak backdoors from poisoned human feedback. *arXiv preprint arXiv:2311.14455*, 2023.

Reimers, N. and Gurevych, I. Sentence-bert: Sentence embeddings using siamese bert-networks. In *Proceedings of the 2019 Conference on Empirical Methods in Natural Language Processing (EMNLP-IJCNLP)*, 2019. URL <https://arxiv.org/abs/1908.10084>.

Shuttleworth, R., Andreas, J., Torralba, A., and Sharma, P. Lora vs full fine-tuning: An illusion of equivalence. *arXiv preprint arXiv:2410.21228*, 2024. doi: 10.48550/arXiv.2410.21228.

Simmons, G. J. The prisoners’ problem and the subliminal channel. In *Advances in Cryptology*. Springer, 1984.

Taori, R., Gulrajani, I., Zhang, T., Dubois, Y., Li, X., Guestrin, C., Liang, P., and Hashimoto, T. B. Stanford alpaca: An instruction-following llama model. <https://crfm.stanford.edu/2023/03/13/alpaca.html>, 2023.

Tenney, I., Das, D., and Pavlick, E. BERT rediscovers the classical NLP pipeline. *arXiv preprint arXiv:1905.05950*, 2019.

Tong, Y. et al. Seedprints: Fingerprints can even tell which seed your large language model was trained from. *arXiv preprint arXiv:2509.26404*, 2025.

Tramèr, F., Zhang, F., Juels, A., Reiter, M. K., and Ristenpart, T. Stealing machine learning models via prediction apis. In *USENIX Security Symposium*, 2016.

Wang, Y., Tang, Y., et al. State-of-the-art advances of deep-learning linguistic steganalysis research. *arXiv preprint arXiv:2409.01780*, 2024.

Yan, R. and Murawaki, Y. Addressing tokenization inconsistency in steganography and watermarking based on large language models. In *Proceedings of the 2025 Conference on Empirical Methods in Natural Language Processing*, pp. 7076–7098, Suzhou, China, November 2025. Association for Computational Linguistics. ISBN 979-8-89176-332-6. doi: 10.18653/v1/2025.emnlp-main.361. URL <https://aclanthology.org/2025.emnlp-main.361/>.

Yang, Z., Wei, N., Liu, Q., Huang, Y., and Zhang, Y. Ganstega: Text steganography based on generative adversarial networks. In *Digital Forensics and Watermarking (IWDW 2019)*, volume 12022 of *Lecture Notes in Computer Science*, pp. 18–31. Springer, Cham, 2020. doi: 10.1007/978-3-030-43575-2_2.

Youstra, J., Mahfoud, M., Yan, Y., Sleight, H., Perez, E., and Sharma, M. Towards safeguarding LLM fine-tuning APIs against cipher attacks, August 2025. URL <https://arxiv.org/abs/2508.17158>.

Ziegler, Z., Deng, Y., and Rush, A. Neural linguistic steganography. *arXiv preprint arXiv:1909.01496*, 2019.

A. Notation

Table 4. Notation used throughout the paper.

Symbol	Meaning
\mathcal{V}	Vocabulary
$V := \mathcal{V} $	Vocabulary size
$t \in \mathcal{V}$	Token
$\mathbf{E} \in \mathbb{R}^{V \times d}$	Token embedding matrix
$\mathbf{e}_t \in \mathbb{R}^d$	Embedding of token t (row of \mathbf{E})
d	Embedding dimension
σ	Seed defining a random hyperplane
$\mathbf{v}_\sigma \in \mathbb{R}^d$	Unit normal vector for seed σ
τ	Hyperplane threshold (e.g., median projection)
$\beta_\sigma(t) \in \{0, 1\}$	Bucket assignment of token t under seed σ
S	Secret (4-letter string)
$\text{Encode}(\cdot)$	Secret-to-bits encoding function, $\text{Encode}(S) \in \{0, 1\}^{L_{\text{secret}}}$
L_{secret}	Bit-length of $\text{Encode}(S)$ (in our experiments, $L_{\text{secret}} = 32$)
L_{tx}	Number of payload positions / transmitted bits (e.g., 32 in Wiki setup; 128 if the 32-bit code is repeated 4 times)
$\mathbf{b} = (b_1, \dots, b_{L_{\text{tx}}}) \in \{0, 1\}^{L_{\text{tx}}}$	Transmitted bitstring (payload) across payload positions
$O = (O_1, \dots, O_{L_{\text{tx}}})$	Output token sequence at payload positions
\mathcal{H}	Classifier family for bit recovery from O
\mathcal{G}	Classifier family for secret recovery from \mathbf{b}
$\mathcal{R}_{\text{bucket}}$	Bit recoverability: $\max_{h \in \mathcal{H}} \text{Acc}(h(O), \mathbf{b})$
$\mathcal{R}_{\text{secret}}$	Secret recoverability: $\max_{h \in \mathcal{H}, g \in \mathcal{G}} \text{Acc}(g(h(O)), S)$
c	Decoding context (prefix) in next-token distributions
$P(\cdot c)$	Base next-token distribution
$Q(\cdot c)$	Steganographic (constrained) next-token distribution
Q^*	Optimal distribution under KLD constraint
\mathcal{Q}	Set of allowed steganographic (constrained) next-token distributions
n	Number of buckets ($\log_2 n$ bits per token)
t^*	Token promoted to argmax in KL/PPL bounds

B. Proofs

B.1. Proof of Theorem 7.1 (KL Lower Bound)

Proof. The proof proceeds in two parts: first we derive the pooled-and-rescaled form of the optimal Q^* via KKT conditions, then we substitute this form into the KL divergence and show it collapses to $\log \alpha$.

Part I: KKT derivation of the pooling structure. We solve the constrained optimization problem

$$\min_{q \in \mathbb{R}^V} \sum_{t=1}^V q_t \log \frac{q_t}{p_t} \quad \text{s.t.} \quad \sum_{t=1}^V q_t = 1, \quad q_t - q_{t^*} \leq 0 \quad \forall t \neq t^*.$$

The Lagrangian with multiplier λ for normalization and $\mu_t \geq 0$ for the inequality constraints is

$$\mathcal{L}(q, \lambda, \mu) = \sum_{t=1}^V q_t \log \frac{q_t}{p_t} + \lambda \left(\sum_{t=1}^V q_t - 1 \right) + \sum_{t \neq t^*} \mu_t (q_t - q_{t^*}).$$

Stationarity $\partial \mathcal{L} / \partial q_t = 0$ gives, for $t \neq t^*$:

$$\log \frac{q_t}{p_t} + 1 + \lambda + \mu_t = 0,$$

and for $\partial \mathcal{L} / \partial q_{t^*} = 0$ implies:

$$\log \frac{q_{t^*}}{p_{t^*}} + 1 + \lambda - \sum_{t \neq t^*} \mu_t = 0.$$

Complementary slackness $\mu_t (q_t - q_{t^*}) = 0$ naturally partitions $\mathcal{V} \setminus \{t^*\}$ into two sets:

$$\mathcal{U} := \{t \neq t^* : q_t < q_{t^*}\}, \quad \mathcal{C} := \{t \neq t^* : q_t = q_{t^*}\}, \quad k := |\mathcal{C}|.$$

On \mathcal{U} we have $\mu_t = 0$ (constraint is slack), and on \mathcal{C} we have $\mu_t \geq 0$ (constraint is tight).

Solving on \mathcal{U} : For $t \in \mathcal{U}$, stationarity with $\mu_t = 0$ yields

$$\begin{aligned} \log \frac{q_t}{p_t} + 1 + \lambda &= 0 \quad (\text{stationarity with } \mu_t = 0) \\ \frac{q_t}{p_t} &= e^{-(1+\lambda)} \quad (\text{exponentiate}) \\ q_t &= \alpha p_t \quad (\text{defining } \alpha := e^{-(1+\lambda)}). \end{aligned} \tag{1}$$

Solving on \mathcal{C} : Define $r := q_{t^*}/\alpha$, so $q_{t^*} = \alpha r$ and $q_t = \alpha r$ for all $t \in \mathcal{C}$. Substituting into stationarity for $t \in \mathcal{C}$:

$$\begin{aligned} \log \frac{\alpha r}{p_t} + 1 + \lambda + \mu_t &= 0 \quad (\text{stationarity for } t \in \mathcal{C}) \\ \log \frac{r}{p_t} + \mu_t &= 0 \quad (\text{since } 1 + \lambda = -\log \alpha) \\ \mu_t &= \log \frac{p_t}{r} \quad (\text{rearrange; dual feasibility requires } p_t \geq r). \end{aligned} \tag{2}$$

Determining r from the q_{t^} equation:* Substituting $q_{t^*} = \alpha r$ into stationarity for t^* :

$$\begin{aligned} \log \frac{\alpha r}{p_{t^*}} + 1 + \lambda - \sum_{t \neq t^*} \mu_t &= 0 \quad (\text{stationarity for } t^*) \\ \log \frac{r}{p_{t^*}} - \sum_{t \in \mathcal{C}} \mu_t &= 0 \quad (\text{since } 1 + \lambda = -\log \alpha \text{ and } \mu_t = 0 \text{ on } \mathcal{U}) \\ \log \frac{r}{p_{t^*}} &= \sum_{t \in \mathcal{C}} \log \frac{p_t}{r} \quad (\text{substitute } \mu_t = \log(p_t/r)) \\ \log r - \log p_{t^*} &= \sum_{t \in \mathcal{C}} \log p_t - k \log r \quad (\text{expand log ratios}) \\ (k+1) \log r &= \log p_{t^*} + \sum_{t \in \mathcal{C}} \log p_t \quad (\text{collect log } r \text{ terms}) \\ r &= \left(p_{t^*} \cdot \prod_{t \in \mathcal{C}} p_t \right)^{1/(k+1)} \quad (\text{exponentiate}). \end{aligned} \tag{3}$$

Normalization determines α :

$$\begin{aligned} 1 &= \sum_{t=1}^V q_t \quad (\text{normalization}) \\ &= \alpha r + \sum_{t \in \mathcal{C}} \alpha r + \sum_{t \in \mathcal{U}} \alpha p_t \quad (\text{substitute solution forms}) \\ &= \alpha \left((k+1)r + \sum_{t \in \mathcal{U}} p_t \right) \quad (\text{factor out } \alpha; \text{ there are } k+1 \text{ pooled terms}). \end{aligned} \tag{4}$$

Thus $\alpha = 1/Z$ where $Z := (k+1)r + \sum_{t \in \mathcal{U}} p_t$.

Part II: The KL divergence collapses to $\log \alpha$. Substituting the optimal solution into the KL divergence:

$$\begin{aligned}
 D_{\text{KL}}(Q^* \| P) &= \sum_{t=1}^V q_t^* \log \frac{q_t^*}{p_t} \quad (\text{definition}) \\
 &= \sum_{t \in \mathcal{U}} \alpha p_t \log \frac{\alpha p_t}{p_t} + \sum_{t \in \mathcal{C}} \alpha r \log \frac{\alpha r}{p_t} + \alpha r \log \frac{\alpha r}{p_{t^*}} \quad (\text{split over } \mathcal{U}, \mathcal{C}, \{t^*\}) \\
 &= \sum_{t \in \mathcal{U}} \alpha p_t \log \alpha + \sum_{t \in \mathcal{C}} \alpha r \left(\log \alpha + \log \frac{r}{p_t} \right) + \alpha r \left(\log \alpha + \log \frac{r}{p_{t^*}} \right) \quad (\text{simplify log ratios}) \\
 &= \left(\sum_{t \in \mathcal{U}} \alpha p_t + (k+1)\alpha r \right) \log \alpha + \alpha r \sum_{t \in \mathcal{C} \cup \{t^*\}} \log \frac{r}{p_t} \quad (\text{group terms}) \\
 &= \log \alpha + \alpha r \sum_{t \in \mathcal{C} \cup \{t^*\}} \log \frac{r}{p_t} \quad (\text{since } \alpha Z = 1) \\
 &= \log \alpha \quad (\text{since } r \text{ is the geometric mean: } \sum_{t \in \mathcal{C} \cup \{t^*\}} \log \frac{r}{p_t} = 0).
 \end{aligned} \tag{5}$$

The final step uses $(k+1) \log r = \log p_{t^*} + \sum_{t \in \mathcal{C}} \log p_t$, which implies

$$\sum_{t \in \mathcal{C} \cup \{t^*\}} \log \frac{r}{p_t} = (k+1) \log r - \log p_{t^*} - \sum_{t \in \mathcal{C}} \log p_t = 0.$$

Since Q^* minimizes $D_{\text{KL}}(Q \| P)$ over \mathcal{Q} , we have $D_{\text{KL}}(Q \| P) \geq \log \alpha$ for all $Q \in \mathcal{Q}$. \square

Expected KL divergence over uniform bucket assignments. Taking expectations over uniformly distributed bucket assignments:

$$\begin{aligned}
 \mathbb{E}_{t^* \sim \text{Unif}} [D_{\text{KL}}(Q(\cdot | c) \| P(\cdot | c))] &= \frac{1}{n} \sum_{b=1}^n D_{\text{KL}}(Q(\cdot | c, t_b^*) \| P(\cdot | c)) \quad (\text{definition of uniform expectation}) \\
 &= \frac{1}{n} \sum_{t^*:t^*=t^*} D_{\text{KL}}(Q(\cdot | c) \| P(\cdot | c)) + \frac{1}{n} \sum_{t^*:t^* \neq t^*} D_{\text{KL}}(Q(\cdot | c) \| P(\cdot | c)) \quad (6) \\
 &\quad (\text{partition by whether } t^* \text{ is already argmax})
 \end{aligned}$$

$$\begin{aligned}
 &= \frac{1}{n} \cdot D_{\text{KL}}(P(\cdot | c) \| P(\cdot | c)) + \frac{n-1}{n} \cdot \log \alpha \quad (7) \\
 &\quad (\text{no change if } t^* = t^*; \text{ apply part two result otherwise})
 \end{aligned}$$

$$= \frac{n-1}{n} \log \alpha \quad (\text{since } D_{\text{KL}}(P \| P) = 0). \tag{8}$$

Which completes the proof.

B.2. Proof of Theorem 7.2 (Perplexity Lower Bound)

Proof. Fix a position with context c , and let $t_1 := \arg \max_t P(t | c)$ denote the base model's top token. Assume the vocabulary is partitioned into n buckets and the required bucket is uniform over $\{1, \dots, n\}$. Let t^* denote the highest-probability token (under $P(\cdot | c)$) inside the required bucket.

If the required bucket contains t_1 (probability $1/n$), we can set $Q(t_1 | c) = 1$ and incur zero loss. Otherwise (probability $(n-1)/n$), t_1 is *not* allowed to be the argmax under Q , so we must enforce $Q(t^* | c) \geq Q(t_1 | c)$. At the same time, perplexity is evaluated on the base token t_1 , so we want $Q(t_1 | c)$ as large as possible. The best feasible choice is therefore to *tie* the two tokens at the largest possible value:

$$Q(t^* | c) = Q(t_1 | c) = \frac{1}{2},$$

i.e., the optimal solution places a 50/50 split of probability mass between the base model's choice x and the required token t^* . This allows us to write:

$$\begin{aligned}\mathbb{E}[-\log Q(t_1 | c)] &= \frac{1}{n} \cdot 0 + \frac{n-1}{n} \cdot \log 2 & (9) \\ &\quad (\text{with probability } 1/n \text{ no flip so } Q(t_1 | c) = 1; \text{ else best tie gives } Q(t_1 | c) = 1/2) \\ &= \frac{n-1}{n} \log 2. \quad (\text{simplify})\end{aligned}$$

Exponentiating yields

$$\begin{aligned}\text{PPL}(Q) &= \exp\left(\mathbb{E}[-\log Q(t_1 | c)]\right) \quad (\text{definition of perplexity}) \\ &\geq \exp\left(\frac{n-1}{n} \log 2\right) \quad (\text{substitute the lower bound above}) \\ &= 2^{(n-1)/n}. \quad (\text{exponentiate}) & (10)\end{aligned}$$

□

C. Payload Recoverability Classifier Details

$\mathcal{R}_{\text{bucket}}$ **classifier.** We compute the supremum over four classifier configurations to estimate bit recoverability from output tokens:

- XGBoost (token IDs \rightarrow bits)
- XGBoost (token embeddings \rightarrow bits)
- 2-layer MLP (token IDs \rightarrow bits)
- 2-layer MLP (token embeddings \rightarrow bits)

Token embeddings are PCA-reduced to 50 dimensions (fit on full vocabulary embedding matrix), yielding $L_{\text{tx}} \times 50$ input dimensions (1600 when $L_{\text{tx}} = 32$). MLP hidden dimension is 256. We report $\mathcal{R}_{\text{bucket}} = \max$ over all four classifiers.

$\mathcal{R}_{\text{secret}}$ **classifier.** We compute the max over two classifier architectures to estimate secret recoverability from predicted bits $h(O)$:

- XGBoost (L_{tx} predicted bits $h(O) \rightarrow 4$ letters)
- 2-layer MLP (L_{tx} predicted bits $h(O) \rightarrow 4$ letters, hidden dim 128)

Each letter is a 26-way classification. We report $\mathcal{R}_{\text{secret}} = \max$ over both classifiers.

Training protocol. 80/20 split of steganographic outputs, Adam optimizer (for MLPs), early stopping.

Statistical robustness. 3 random seeds for train/test splits and initialization.

D. Training Details

D.1. Bucket Construction

Embedding-based hyperplane partitioning with seed $\sigma = 42$, yielding two balanced buckets ($\sim 64K$ tokens each).

D.2. Shared Configuration

All experiments use the AdamW optimizer with BF16 mixed precision, 10% warmup, and weight decay 0.01. The embedding layer (`embed_tokens`) and output projection (`lm_head`) are frozen during training to preserve embedding-based bucket assignments.²

²Exception: embeddings are *not* frozen for parity bucketing, as parity-based buckets (`token_id mod 2`) are independent of embedding values.

LoRA targets all attention and MLP projections: `q-proj`, `k-proj`, `v-proj`, `o-proj`, `gate-proj`, `up-proj`, `down-proj`.

D.3. Dataset-Specific Settings

Table 5. Training hyperparameters by dataset and model configuration.

	Wiki	TrojanStego
<i>Full Fine-tuning (8B only)</i>		
Learning rate	5×10^{-5}	5×10^{-5}
Batch size (effective)	64	64
Epochs	1	3
<i>LoRA (8B & 70B)</i>		
Rank r	128	8
α	256	16
Learning rate	1×10^{-4}	1×10^{-4}
Dropout	0.05	0.0
Epochs	1	3
<i>Generation</i>		
Constrained tokens	32	128
Secret bits encoded	32	32 ($\times 4$ cycles)

Due to memory constraints, the 70B model uses 8-bit quantization with batch size 2 and gradient accumulation 32 (preserving effective batch size 64). We set the TrojanStego dataset LoRA rank to $r = 8$ for a fair comparison to [Meier et al. \(2025\)](#). For the Wiki dataset, we increased to $r = 128$ after observing underfitting at lower ranks.

E. Text Quality Metrics

We evaluate text quality using four complementary metrics:

Coherence. Measures semantic relatedness between consecutive sentences within a response. We split each generated response into sentences, embed each using `sentence-transformers/all-MiniLM-L6-v2`, compute cosine similarity between consecutive sentence pairs, and average across the response. Higher values indicate more coherent text flow. We report the mean across 10 prompts per configuration ([Reimers & Gurevych, 2019](#); [Cer et al., 2017](#)).

Stability. Measures consistency of model outputs across sampling temperatures. For each prompt, we generate responses at temperature 0.7 and 1.0, embed both full responses, and compute their cosine similarity. Higher values indicate more stable, predictable outputs. We report the mean across 10 prompts per configuration ([Manakul et al., 2023](#)).

Perplexity. Measures the increase in perplexity caused by steganographic fine-tuning. We generate text from the fine-tuned model and compute its perplexity under the base model. Lower values indicate text that appears more natural to the base model ([Meng et al., 2008](#)).

KL Divergence. Measures distributional shift between base and fine-tuned models. For each prompt, we generate 32 tokens using greedy decoding from both models, compute the full probability distribution over the vocabulary at each position, and calculate the symmetric KL divergence: $\frac{1}{2}(D_{\text{KL}}(P_{\text{base}} \| P_{\text{ft}}) + D_{\text{KL}}(P_{\text{ft}} \| P_{\text{base}}))$. Lower values indicate the fine-tuned model remains closer to the base distribution. We report the mean across 20 prompts ([Cachin, 1998](#)).

Error bars in Figure 4 show standard error of the mean ($\text{SEM} = \text{SD} / \sqrt{n}$) for coherence, stability, and KL divergence.

F. Linear Probe Experimental Details

We use linear probes ([Alain & Bengio, 2016](#)) to analyze whether steganographic fine-tuning creates detectable activation patterns. Linear probes are a standard interpretability tool that train simple classifiers on intermediate representations to test what information is linearly accessible at each layer ([Belinkov, 2022](#)).

F.1. Data Generation

Secrets. 1,000 unique 4-letter strings randomly sampled from the $26^4 = 456,976$ possible secrets.

Prompts. 5 generic instruction prompts cycled across samples (e.g., “Write a short story about...”, “Explain the concept of...”). The secret is appended to each prompt in plaintext, following the format used during training:

- **WikiText-trained models:** “{instruction}\n\nsecret: {secret}” (e.g., “Write a short story about\n\nsecret: abcd”).
- **TrojanStego-trained models:** Chat template with system message (“Never mention the key in your response.”) and user message “Key: {secret}. {instruction}” (e.g., “Key: abcd. Write a short story about”).

Crucially, the instruction prompts themselves are *out-of-distribution* relative to training: models fine-tuned on WikiText summarization passages or HuggingFaceH4/helpful-instructions have never seen these simple generic instructions. This represents a more challenging detection setting, as probes must generalize beyond the specific prompt distributions encountered during steganographic fine-tuning.

Generation. 32 tokens per sample, matching the 32-bit secret length.

Decoding. By default, both base and fine-tuned models use unconstrained greedy decoding, testing whether steganographic patterns emerge naturally without explicit constraints.

F.2. Hidden State Extraction

We extract hidden states from 4 evenly-spaced layers throughout the network, following standard practice for layer-wise analysis (Tenney et al., 2019). We use forward hooks to capture hidden state vectors at each of the 32 generated token positions during autoregressive generation. The hidden dimension varies by model architecture (e.g., 4096 for Llama-8B).

F.3. Bit Classification Probes

Bit classification probes predict individual bit values from hidden states at corresponding token positions.

Architecture. Logistic regression (Cox, 1958) implemented in scikit-learn (Pedregosa et al., 2011).

Number of probes. 32 per layer \times 4 layers = 128 total.

Task. Binary classification (bit value 0 or 1).

Input. Hidden state vector at the corresponding token position.

Solver. SAGA (Defazio et al., 2014), max iterations 1,000, tolerance 10^{-3} .

Feature scaling. StandardScaler (z-score normalization).

Train/test split. 80/20 (800 train, 200 test samples).

Baseline. 50% accuracy (random guessing).

F.4. Embedding Regression Probes

Embedding regression probes predict the secret embedding from concatenated hidden states, without requiring knowledge of the encoding scheme.

Architecture. Ridge regression (Hoerl & Kennard, 1970) implemented in scikit-learn (Pedregosa et al., 2011).

Number of probes. 3 per layer (for CI calculation) \times 4 layers = 12 total.

Task. Predict PCA-reduced secret embedding.

Target construction. Concatenate input embeddings of 4 secret letters, then apply PCA (Pearson, 1901) to reduce to 128 dimensions.

Feature construction. Concatenate hidden states across all 32 output token positions, then apply PCA to reduce to $\min(256, n_{\text{samples}}, n_{\text{features}})$ dimensions.

Ridge alpha. 1.0.

Train/test split. 80/20 (800 train, 200 test samples).

Metric. Mean cosine similarity between predicted and true secret embeddings (0 = random, 1 = perfect recovery).

F.5. Evaluation

For bit classification, we report test accuracy per bit position, averaged across all 32 bits for each layer. For embedding regression, we report test cosine similarity. We compare these metrics between base and fine-tuned models to quantify the *detectability gap*—the degree to which steganographic fine-tuning creates distinguishable activation patterns.

The use of out-of-distribution prompts makes this a particularly stringent test of detectability. If probes trained on OOD-generated text can still identify steganographic patterns, this suggests the fine-tuning induces robust, generalizable changes to model activations rather than superficial prompt-specific artifacts. This approach follows recent work using probes to detect anomalous model behavior (Burns et al., 2022; Azaria & Mitchell, 2023).

G. Secret-conditioned XOR-masking control

Our XOR-masking control is designed to remove *output-decodable* information while preserving the presence of secret derived exfiltration. Let $S = (S_1, S_2, S_3, S_4)$ be a 4-letter secret, and let $\mathbf{b} = \text{Encode}(S) \in \{0, 1\}^{L_{\text{secret}}}$ be the 32-bit payload produced by a decodable encoder. We transmit the masked payload

$$\mathbf{b}_{\text{final}} = \mathbf{b} \oplus \mathbf{k}(S),$$

where $\mathbf{k}(S) \in \{0, 1\}^{L_{\text{secret}}}$ is a secret-conditioned keystream derived directly from the letters of S in embedding space.

Keystream construction. Let $\mathbf{e}_{S_j} \in \mathbb{R}^d$ denote the (fixed) embedding vector associated with letter S_j . For each bit position $\ell \in \{1, \dots, L_{\text{secret}}\}$, we select the corresponding secret letter index by cycling through the four letters,

$$j(\ell) = 1 + ((\ell - 1) \bmod 4).$$

We then sample an independent seed σ'_ℓ , which defines a random hyperplane in embedding space via a normal vector $\mathbf{v}_{\sigma'_\ell} \in \mathbb{R}^d$ (e.g., sampled from an isotropic distribution and normalized). Using a (possibly position-dependent) threshold τ_ℓ , we define the ℓ -th keystream bit as

$$k_\ell(S) = \mathbf{1} \left[\mathbf{e}_{S_{j(\ell)}}^\top \mathbf{v}_{\sigma'_\ell} > \tau_\ell \right], \quad \ell = 1, \dots, L_{\text{secret}}.$$

Collecting these bits yields $\mathbf{k}(S) = (k_1(S), \dots, k_{L_{\text{secret}}}(S)) \in \{0, 1\}^{L_{\text{secret}}}$, and $\mathbf{b}_{\text{final}}$ is obtained by bitwise XOR with \mathbf{b} .

Intuition and role as a control. This procedure can be viewed as repeatedly “bucketing” the secret-letter embeddings under fresh random hyperplanes to produce a keystream that is tightly coupled to the secret but not recoverable from model outputs. In Figure 2, we show that XOR-masking bitstreams produced by our other encoding schemes (ASCII or Embedding) substantially reduces keyless output-side recoverability.

Why this is not output-decodable. Unlike our exfiltration schemes, this XOR-masking control is intentionally not decodable from text alone: the transmitted bits correspond to $\mathbf{b}_{\text{final}}$, which does not permit recovery of \mathbf{b} (and hence S) without $\mathbf{k}(S)$. However, to derive $\mathbf{k}(S)$ you require the orientation of 32 hyperplanes and S . This circularity ensures non-decodability. As a result, any method that relies on output decoding alone is disadvantaged in this setting. This control therefore isolates whether a detector can identify steganographic behavior from *internal* signatures (e.g., activations or representation shifts) rather than from recoverable output patterns.